



A new method of processing CO₂ and magnesite slag simultaneously

NA YANG, PING NING*, KAI LI and JUNYA WANG**

Faculty of Environmental Science and Engineering, Kunming University of Science and Technology, Kunming, 650500, Yunnan, P. R. China

(Received 28 May, revised 12 September, accepted 19 September 2018)

Abstract: Calcining magnesite slag to capture CO₂ is a new and simple method of processing CO₂ and magnesite slag simultaneously. In this work, the CO₂ capture capacity by calcined magnesite slag in wet flue gas simulated by adding water vapour was investigated. The magnesite slag exhibits excellent CO₂ adsorption performance, with 3.01 mmol/g CO₂ adsorption capacity, which is reduced to 2.18 mmol/g after 8 cycles and is obvious superior to magnesite. The structure and characterization of the magnesite slag are examined by XRF, FT-IR, TG-DSC, XRD, CO₂-TPD and BET. It can be confirmed by X-ray fluorescence analysis that the key component of magnesite slag is MgSiO₃ and MgCO₃. The results of this work indicate that the magnesite slag is an available adsorbent for CO₂ adsorption after calcination.

Keywords: greenhouse gas; calcined condition; slag; adsorption capacity

INTRODUCTION

Since 2000, many countries have been constantly setting records of high temperature, and the number of days with high temperature continues to increase. The degree of the global warming has more than that in the past. The global environment will undergo a major change, and these changes will change the life of the people in different forms. Countries have begun to take measures of energy conservation and emissions reduction to slow the climate change process. The carbon capture and sequestration (CCS) technology was proposed and considered to be one of the major solutions to mitigate greenhouse problems internationally, intending to reduce 20 % emission by 2020¹. The methods to capture CO₂ mainly include pre-combustion capture, post-combustion, oxy-combustion capture and others. The existing technology has physical absorption separation, adsorption separation, membrane separation, cryogenic distillation and absorption, emerging of oxygen-enriched combustion and chemical chain combustion technology, etc.

*,** Corresponding authors. E-mail: (*)452498425@qq.com; (**junyawang@kmust.edu.cn
<https://doi.org/10.2298/JSC180528077Y>

There are more and more reports on separation by adsorption, due to the advantages of regeneration and convenient industrial application, while the important issues for the methods is to develop a non-polluting and efficient adsorbent.² Researchers have developed ionic liquids,³ MOFs,⁴ alkali metal oxide,⁵ activated carbon⁶ and porous materials⁷ for CO₂ capture, obtaining some achievements. Many new materials also appear constantly. Alkali metal and alkaline oxide, especially MgO, CaO based sorbents, are investigated mostly due to the abundant sources, low cost, as well as non-toxicity.⁸ However, MgO based adsorbents need lower regeneration temperature than CaO based types, so MgO has advantages in regenerating MgCO₃ to MgO. Many investigations on MgO based adsorbents were reported, MgO/Al₂O₃,⁹ mesoporous MgO,¹⁰ MgO–TiO₂,¹¹ MgO–SiO₂,¹² MgO–C,¹³ MgO–ZrO₂,¹⁴ and so on.^{15–19} In addition, the cyclic CO₂ removal process based on MgO type sorbents was proposed to perform the circulation.

We investigated the CO₂ adsorption performance by magnesite in previous work.²⁰ Thus, we proposed if the slag could be used in CO₂ capture, as it was a sort of waste from the process of magnesite smelting to achieve metal Mg by Si-thermal-reduction method, also contained MgO, CaO, SiO₂ and other alkaline oxide, which have CO₂ adsorption performance. As the result, it exhibited better CO₂ adsorption performance. As the continuation of the previous work, we investigated the CO₂ adsorption performance of magnesite slag in the same experimental setup and the methodology of the investigation and compared the CO₂ performance with the magnesite. The obvious difference and advantage of this paper from the previous work lie that not only CO₂, but also a waste is processed. Applying magnesite slag in the CO₂ capture can not only reduce greenhouse gas emission, but also comprehensively utilize industrial waste residue, with advantages of abundant source, no pollution, low cost and recycling easily.²¹

EXPERIMENTAL

Chemical reagents and devices

CO₂ (N₂ as balance gas) with 10 % volume fraction and N₂ with a purity of 99.999 % were bought from Dalian Gas Co. Ltd. The magnesite slag was supplied by Shandong Laizhou Magnesium mine. Gas mass flow controllers (D08-1D/ZM for 99.999 % N₂; D08-1F for 10 % CO₂) were produced by Beijing Sevenstar electronics Co.,Ltd. Infrared gas analyzer (ANT-ARIS IGS analyzer) was purchased from Thermo Scientific Instrument Co.,Ltd. Muffle furnace was produced by BangXi Technology Instrument Co.,Ltd., One-way valve, three-way valve and counterbalance valve were produced by Beijing Jiafa International Co., Ltd. Circulating water bath pot (CS601) was produced by Shanghai Boxun Instrument Co., Ltd. Electric heating (DF-101S) was supplied by Henan Yuhua Instrument Co., Ltd. Powder compressing machine (769YP-15A), were supplied by Tianjin Keqi Instrument Co., Ltd. Water vapour reactor and absorber were supplied by Yunnan Taifei Instrument Co., Ltd.

CO₂ adsorption and desorption test

Calcining abundant, low cost and non-pollution magnesite slag in muffle furnace can produce MgO-based adsorbent for CO₂ capture quite simply. The effects of different calcining

temperature and time controlled by muffle furnace were investigated. CO₂ adsorption experiment chart is shown in Fig. 1. At first the infrared gas analyzer was purged by N₂ with a flow rate 100 mL/min for 15 min. To simulate the real flue gas from industry, 10 % CO₂ with a certain flow rate and steam from water vapour reactor were mixed to replace the gas in the path through the empty branch. After the flow steady, 10 % CO₂ in the present water vapour passed through 3 g adsorbent in the absorber, by adjusting the three-way valve. Then, the infrared gas analyzer stared to detect. The adsorption temperature and pressure were controlled by circulating water bath pot and counterbalance valve. In order to prevent the water vapour condensation, the pipe between water vapour reactor and absorber should be as short as possible and preserve heat by insulation belt. CO₂ desorption experiments were carried out by heating at 550 °C for 4 h with N₂ purging.

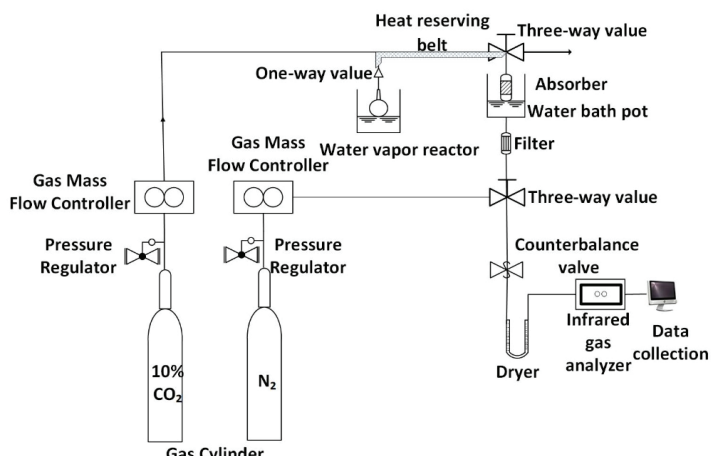


Fig. 1. CO₂ adsorption experiment chart.

Characterization

TG-DSC analyses were performed on a SDT Q600 simultaneous thermal analyzer (TA Corp., USA). The analytical composition of the adsorbent was determined by XRF analysis, using AXIOS wavelength dispersive X-ray fluorescence spectrometer, (PANalytical B.V. Corp., The Netherlands). XRD was carried out on D/MAX-rA instrument (Rigaku Corp., Japan). FT-IR spectra were recorded on a ALPHA-T Fourier Transform Infrared Spectrometer (BRUKER Corp., Germany). The BET surface areas, and porosity analysis were achieved by N₂ adsorption/desorption using Tristar 3020 physisorption apparatus (Micromeritics Corp., USA). The basicity of the adsorbent was measured by CO₂-TPD using Belcat apparatus (Micortrac Bel Corp., USA).

RESULTS AND DISCUSSION

The influence of calcination temperature and time

In order to confirm the calcination temperature range, TG-DSC analyses of the magnesite slag was investigated to provide the basis for the study of the calcination temperature influence, shown in Fig. 2. From Fig. 2, four loss weight peaks can be seen. The first three peaks from 31 to 430 °C with weight loss 0.7,

0.7 and 1.6 % may be due to the loss of small molecules and the decomposition of impurities. The fourth one with weight loss 37.6 % appeared from 430 to 780 °C is due to the decomposition of the magnesite slag, with a DSC endothermic peak.

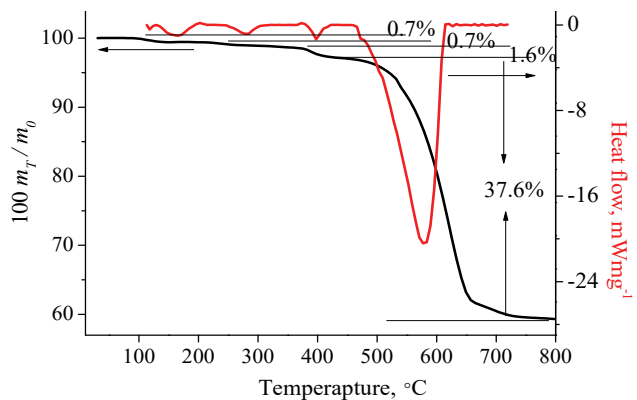


Figure 2. TG-DSC curve of the magnesite slag; m_T : mass at temperature T ; m_0 : initial mass.

To obtain the optimal calcination condition, the calcining temperature and time were investigated. Fig. 3 shows the curves of magnesite slag (3 g) on CO₂ capture performance at different calcination temperature for 5 h under adsorption condition of 60 °C, 0.1 MPa, 100 mL/min flow rate, in the presence of water vapour.

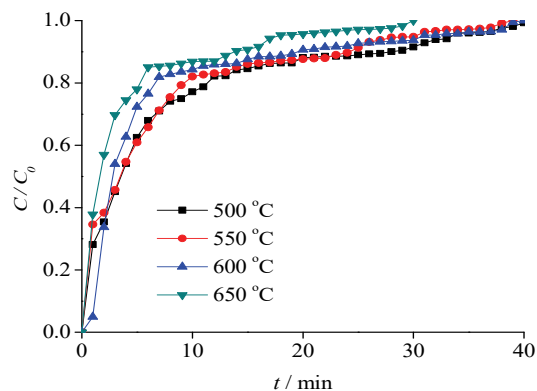


Fig. 3. Adsorption curves at different calcination temperature (3 g, 100 mL min⁻¹, 60 °C, 0.1 MPa; C : the detected concentration, C_0 : the initial concentration).

It indicates that with the calcination temperature increasing, the time to equilibrium shortens gradually, and CO₂ adsorption efficiency shows a decline tendency. The CO₂ capacities under different conditions calculated by the curves are listed in Table I. It can be found that 500 °C is the optimal temperature with CO₂ capacity 1.16 mmol/g, which is chosen to investigate the influence of calcination time, shown in Fig. 4. It can be seen that the adsorption time for the samples calcined for 5 and 6 h were nearly the same, longer than for those

calcined for 3 and 4 h. By the above results and considering the energy consumption, 500 °C and 5 h was enough to make the magnesite slag decompose to MgO, with CO₂ adsorption capacity 1.16 mmol/g. In our previous work, the magnesite for CO₂ capture was calcined at 550 °C for 4 h, and the CO₂ adsorption performance also decreased with higher temperature and longer time.²² The reasons are similar and due to that sintering can occur easily if calcination temperature is too high or time is too long, leading to BET surface area reducing and the pore structure destroyed, which hinders the diffusion of CO₂ in the sorbent particles and decreases the CO₂ adsorption capacity and efficiency.²² That is also the reason why the CO₂ capacity declines with calcination temperature rising. Because of the different ingredient, the calcining time and temperature of magnesite slag have a slight distinction from magnesite. From the energy point of view, there are no significant differences between materials.

TABLE I. CO₂ capacity of magnesite slag under different conditions (10 % CO₂)

Calcination temperature, °C	Calcination time, h	Adsorption temperature, °C	Flow rate mL/min	Adsorption pressure, MPa	CO ₂ adsorption capacity, mmol/g
500	5	60	100	0.1	1.16
550	5	60	100	0.1	1.04
600	5	60	100	0.1	0.97
650	5	60	100	0.1	0.62
500	3	60	100	0.1	0.84
500	4	60	100	0.1	0.89
500	6	60	100	0.1	1.13
500	5	40	100	0.1	0.88
500	5	80	100	0.1	1.43
500	5	100	100	0.1	1.07
500	5	80	150	0.1	1.11
500	5	80	200	0.1	1.08
500	5	80	150	0.4	2.12
500	5	80	150	0.8	3.01

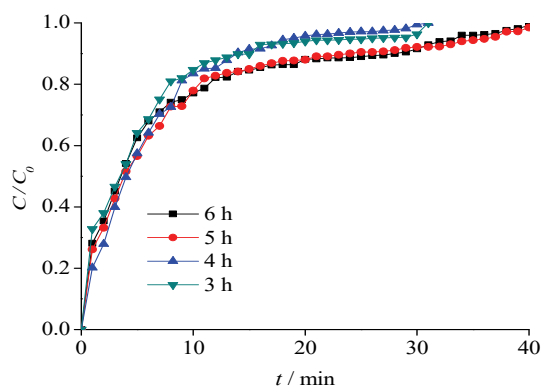


Fig. 4. Adsorption curves, C_0 : under different calcination time (3 g, 100 mL min⁻¹, 60 °C, 0.1 MPa; C : the detected concentration the initial concentration).

The influence of adsorption temperature

Generally, the temperature of exhaust gas from a coal fired power plant is about 100 °C. Through a wet desulfurization unit, it would be around 50 °C.^{23,24} Therefore, the magnesite slag for CO₂ capture in this temperature range was investigated. The magnesite calcined at 500 °C for 5 h was chosen to investigate the CO₂ adsorption performance at 40, 60, 80 and 100 °C. From Fig. 5, it is seen that in the first 10 min, the CO₂ adsorption efficiency increased with the adsorption temperature, and afterwards it remains slightly higher at 80 °C than at other temperatures, with CO₂ capacity 1.43 mmol/g (Table I). It was 1.07 mmol/g at 100 °C, which showed the stable adsorption performance in the temperature range. On the one side, water vapour condensation can make CO₂ adsorb on the surface of adsorbent easily; on the other side, the excessive water vapour condensation restrains CO₂ going through the pipe. At low temperature, there is too much water vapour condensation; at high temperature, there is not enough water vapour condensation on the surface, which explains that the CO₂ adsorption capacities at 60 and 80 °C are larger than that at 40 and 100 °C. In addition, the process includes physical adsorption and chemical adsorption. Increasing temperature can not only reduce physical adsorption and strengthen chemical adsorption, but can also improve the adsorption ratio. From the above, the effect of temperature is complex, and the calcined magnesite slag shows excellent CO₂ adsorption performance in the temperature range of 60–100 °C.

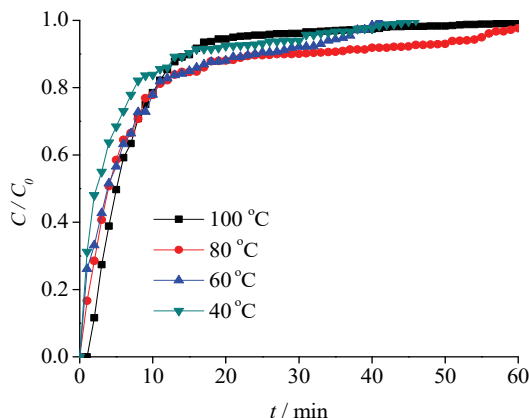


Fig. 5. Adsorption curves at different adsorption temperature (3 g, 100 mL min⁻¹, 0.1 MPa; C: the detected concentration, C_0 : the initial concentration).

The influence of flow rate

In order to improve the adsorption efficiency for industrial application, we studied the effect of flow rate on CO₂ adsorption performance. Fig. 6 indicates the adsorption curves of magnesite slag at 80 °C under different flow rates. It took more than 18 min to reach equilibrium under 100 mL/min flow rate, with CO₂ capacity 1.43 mmol/g, which was decreased with the flow rate increasing

and 10 min were enough for that of 200 mL/min. From Table I, it was found that though the mass transfer was enhanced with flow rate enhanced from 100 to 200 mL/min, CO₂ the adsorption capacity decreased because the contact time of gas and adsorbent shortened. Considering the equilibrium time and industrial application, 150 mL/min flow rate with CO₂ capacity 1.11 mmol/g was chosen in the next experiments.

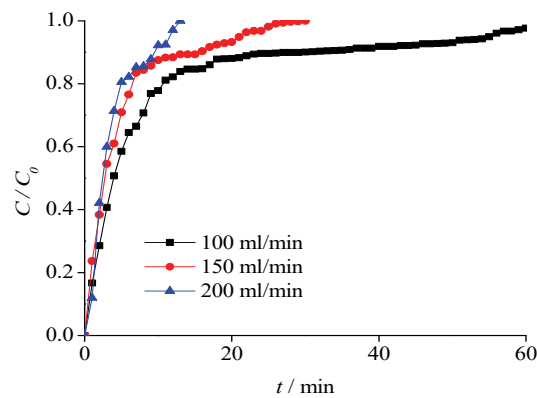


Fig. 6. Adsorption curves at different flow rate (3 g, 80 °C, 0.1 MPa; C : the detected concentration, C_0 : the initial concentration).

The influence of adsorption pressure

We studied the effect of pressure on the CO₂ adsorption performance by the calcined magnesite slag to improve CO₂ adsorption capacity. Fig. 7 indicates the CO₂ adsorption curves of magnesite slag at 80 °C, 150 mL/min flow rate, under the pressure of 0.1, 0.4 and 0.8 MPa, which shows that the pressure increase makes the time to equilibrium extend obviously.

When the pressure reached 0.8 MPa, 3.01 mmol/g CO₂ adsorption capacity was achieved. From the above results, the pressure has an obvious effect on CO₂ adsorption capacity by the magnesite slag. Magnesite was investigated at 0.4 MPa, 100

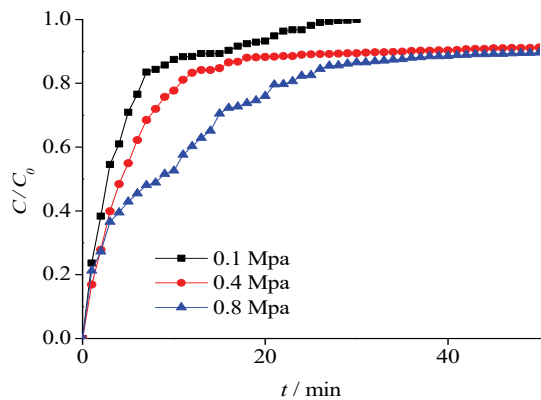


Fig. 7. Adsorption curves at different adsorption pressure (3 g, 150 mL/min, 80 °C; C : the detected concentration, C_0 : the initial concentration).

mL/min 10 % CO₂ flow rate in the presence of water vapour,²⁰ indicating that the slag as a waste, has more advantages in CO₂ capture. By comparing with the CO₂ adsorption capacity reported in literatures listed in Table S-I of the Supplementary material to this paper, our results show slightly advantage, and the calcined magnesite slag is easier to obtained and cheaper than others.

Regeneration of the adsorbent

In order to perform the industrial application, experiments were carried out to examine the regeneration of magnesite slag under the desorption condition 550 °C for 4 h with a purge gas of N₂, the adsorption condition of 80 °C, 0.8 MPa, 150 mL/min flow rate. As shown in Fig. 8, CO₂ adsorption capacity had a slightly decline for the first three repetitive runs and gradually reduced with the following recycling. It still kept 2.18 mmol/g at the eighth cycle, implying the excellent cycle stability.

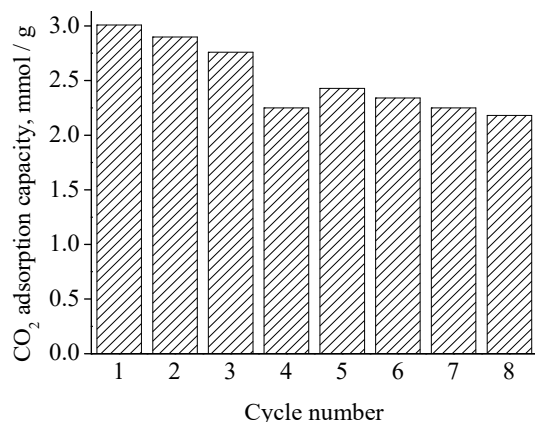


Fig. 8. CO₂ capacity of magnesite slag in 8 cycles (3 g, 150 mL/min, 80 °C, 0.8 MPa).

Comparing the results of magnesite slag to the magnesite (Table S-II of the Supplementary material), it was found that the calcined magnesite achieved CO₂ adsorption capacity 1.82 mmol/g, under the optimal condition of 60 °C, 100 mL/min flow rate. The slag got 2.12 mmol/g CO₂ adsorption capacity under the condition of 80 °C, 0.4 MPa, 150 mL/min flow rate, and reach 3.01 mmol/g when the pressure increased to 0.8 MPa. The CO₂ adsorption performance of slag was obvious superior to magnesite.

Characterization

To determine the ingredient of magnesite slag and the decomposition degree after calcined, XRF analysis was carried out. As shown in Table S-II, high proportion elements of magnesite slag calcined at 500 °C for 5 h include 32.18 % Mg, 11.09 % Si, 3.82 % Al, 3.18 % Mn, 1.51 % Ca and 1.19 % Fe. Analyzing the results, it can be deduced that the corresponding oxides are 53.63 % MgO, 23.76

% SiO₂, 7.22 % Al₂O₃, 4.10 % MnO, 2.1 % CaO and 1.7 % Fe₂O₃. The ratio of MgO and SiO₂ is much larger than that MgSiO₃, indicating the existence of MgCO₃ in magnesite slag. The main composition of the magnesite slag is MgSiO₃ in theory, but a lot of MgCO₃ from the residual magnesite in smelting process also exists. MgO can be achieved by calcining the magnesite slag. Comparing the XRF results of magnesite and slag (Table S-II), it can be seen that the composition is different obviously. From the experimental results, it can be seen that CO₂ adsorption performance is superior to magnesite. Thus, the utilization of MgO in slag is high, which may be due to the assistance of SiO₂, Al₂O₃ and CaO.

In order to study the effect of calcination time on the structure of magnesite slag and the structure of calcined magnesite slag adsorbed CO₂, XRD analysis was performed. The XRD comparisons of the magnesite slag calcined at 3, 4, 5 and 6 h and after CO₂ adsorption are listed in Fig. 9 to confirm the influence of calcination time and whether there are new species generated after adsorbing CO₂. The characteristic diffraction peaks of cubic MgCO₃ were 32.9, 42.9, 53.9, 62.3 and 78.6°,¹² while 32.9 and 42.9° were the diffraction peaks of CO₃²⁻ including CaCO₃, which indicated the uniform cubic crystal structure and single phase of the magnesite slag calcined at 500 °C for different times. However, with the calcined time extending, the peak at 53.9° weakened gradually and disappeared when the magnesite slag calcined for 5 h, proving that the magnesite slag decomposed completely calcined at 500 °C for 5 h. After CO₂ adsorption, the peak at 53.9° appeared again and the peaks at 32.9 and 42.9° were more intense, due to the formation of MgCO₃. Comparing with the XRD patterns of the adsorbent after CO₂ adsorption and the magnesite slag calcined at 500 °C for 3 h

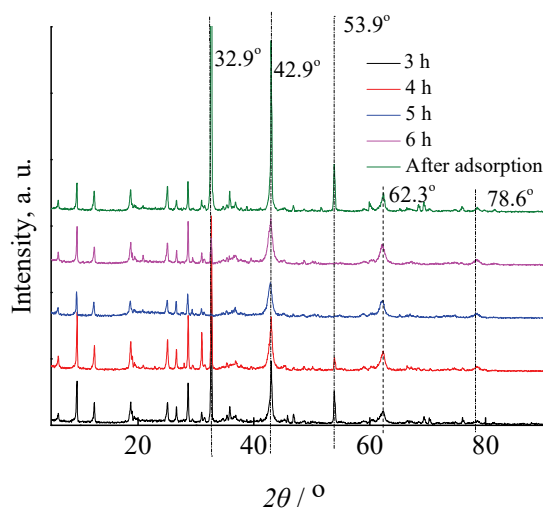


Fig. 9. XRD results of the calcined magnesite slag at 500 °C for different time and the CO₂ adsorbed magnesite slag calcined at 500 °C for 5 h.

with incomplete decomposition, the structure was similar, confirming the existence of MgCO_3 in magnesite slag with the incomplete decomposition, which is consisted with the result of XRF. Before and after adsorption, some other species beyond MgO detected on the XRD patterns had no change, so they did not participate in the adsorption reaction.

The FT-IR spectrum was used to distinguish the functional group before and after CO_2 adsorption, as shown in Fig. 10. The peaks appeared at 860, 1417, 1448 and 1650 cm^{-1} signify the existence of monodentate carbonate, bicarbonate and bidentate carbonate, and the peak at 1820 cm^{-1} is the characteristic peak of carbon and oxygen double bond.^{22,37} From Fig. 10, the peaks of the adsorbent before adsorption appeared at 885, 1436, 1636 and 1820 cm^{-1} display the existence of bidentate carbonate and bicarbonate species involving surface hydroxyl groups, which may be due to the residual little MgCO_3 in the sample. The spectrum after adsorbing CO_2 is similar to that before adsorption, therefore no new species generated. However, the intensity of peaks strengthens, which correlates with the amount of functional group and intrinsic intensity. The peak intensity strengthening showed that the amount of carbonate increased and the magnesite slag adsorbed CO_2 successfully. By FT-IR spectra, it was concluded that the CO_2 adsorbed on calcined magnesite slag was mainly chemisorption.

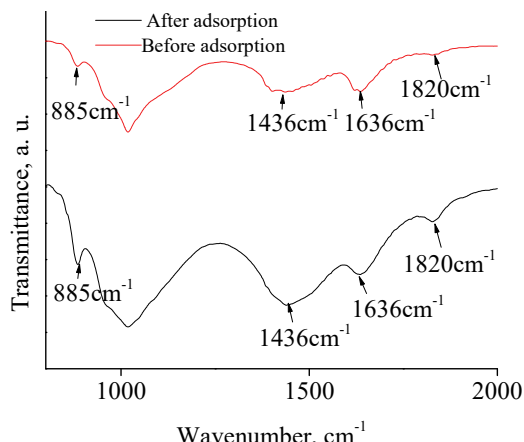


Fig. 10. FT-IR spectra of the calcined magnesite slag at $500\text{ }^\circ\text{C}$ for 5 h before and after CO_2 adsorption.

To check the basicity and the base strength of the calcined magnesite slag at $500\text{ }^\circ\text{C}$ for 3 h and 5 h, CO_2 -TPD at adsorption temperature $80\text{ }^\circ\text{C}$ was performed to confirm the adsorption site. The basicity and base strength of the calcined magnesite slag at $500\text{ }^\circ\text{C}$ for 3 and 4 h were determined by CO_2 -TPD experiments and shown in Fig. 11. The characteristic peaks assigned to the desorption temperatures are indicative of their base strength.

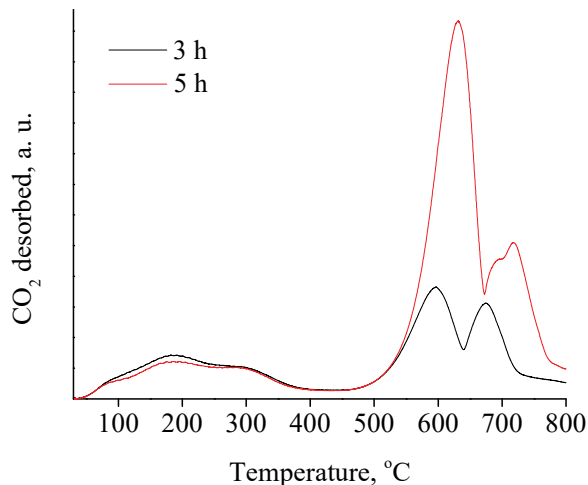


Fig. 11. CO₂-TPD curves of the calcined magnesite slag at 500 °C for 3 h and 5 h (CO₂ adsorption temperature 80 °C).

The desorption peaks at moderate temperature (100–400 °C), standing for weak base sites and medium base sites, were due to the physical adsorption, the weakly chemisorbed CO₂ on the surface hydroxyl groups, in the presence of water vapour, to form bicarbonate and the strongly chemisorbed CO₂ on the Mg²⁺ and O²⁻ in the form of bidentate carbonate. The two peaks between 500 and 800 °C might be ascribed to the strong base sites, most corresponding to the isolated O²⁻.²⁹ The peaks of magnesite slag calcined for 5 h were obviously higher than that 3 h and the results were well in accordance with the calcined temperature time.

Surface area and porosity analysis were used to study the parameters of the porous structure of calcined magnesite slag after cycling. Table II and Fig. S-1 of the Supplementary material showed the BET results and N₂ adsorption–desorption isotherms as well as the pore size distributions.

TABLE II. Porous structure parameters achieved by N₂ adsorption-desorption isotherm

Sample	BET surface area, m ² /g	Pore volume, cm ³ /g	Pore size, Å
Calcined magnesite slag (500 °C)	51.26	0.08	26.39
Calcined magnesite slag (600 °C)	28.03	0.04	27.30
After 4 cycles	26.86	0.05	29.85
After 8 cycles	29.43	0.04	27.42

The results showed that both of the BET surface area and the pore volume of magnesite slag calcined at 600 °C were lower than that 500 °C, due to the sintering occurring at high calcination temperature, which was the reason why the CO₂ adsorption capacity decreased with the calcination temperature increasing. The BET surface area after 4 cycles decreased from 51.26 to 26.86 m²/g, the pore

volume had a slight decreasing from 0.08 to 0.05 cm³/g, and the pore size increased from 26.39 to 29.85 Å, which was caused by calcination and high pressure repeatedly, leading to the CO₂ capacity decrease. After 8 cycles, the BET surface area increased slightly, and the pore volume as well as the pore size decreased, which might be due to the reaction during CO₂ adsorption and desorption. According to the International Union of Pure and Applied Chemistry (IUPAC) classification, from Fig. S-1 it could be seen that the samples showed type IV isotherm with a H3 hysteresis loop, which were characteristics of mesoporous materials (2 nm < pore size < 50 nm). The BET surface area of magnesite is 122.8 m²/g,²⁰ higher than the slag. The superior performance of the slag indicated that its assistance played an important role in CO₂ adsorption performance, though the BET surface area also could influence it.

CONCLUSION

Applying the magnesite slag in the CO₂ capture is a new and simple method that can not only reduce CO₂ emission, but also comprehensively use the industrial waste residue. The experiments results showed that 500 °C for 5 h was enough to make magnesite slag decompose to MgO. CO₂ adsorption capacity 3.01 mmol/g was achieved under the condition of 80 °C, 150 mL/min, 0.8 MPa, and reduced to 2.18 mmol/g after 8 cycles, which was obviously superior to magnesite with 1.82 mmol/g CO₂ adsorption capacity, under the optimal condition of 60 °C, 0.4 MPa, 100 mL/min flow rate. All the results indicated that the calcined magnesite slag had good CO₂ adsorption performance and stability and was a promising adsorbent for CO₂ capture from wet flue gas. The slag obtained as a waste during the metal Mg production, has better performance on CO₂ capture in comparison to magnesite, and the impurities could play an assistant role. However, for industrial application, the future work that needs to be done should be focused on the effect of NO_x, SO_x and others in flue gas on CO₂ adsorption performance of calcined magnesite slag.

SUPPLEMENTARY MATERIAL

Additional experimental results are available electronically at the pages of journal website: <http://www.shd.org.rs/JSCS/>, or from the corresponding author on request.

Acknowledgements. This study was supported by Natural Science Foundation of China (No. 51368026, 51568027, 51568067), the Scientific Researching Fund Projects of Yunnan Provincial Department of Education (2017ZZX137).

И З В О Д

НОВИ ПОСТУПАК ЗА ИСТОВРЕМЕНИ ТРЕТМАН CO₂ И МАГНЕЗИТИНЕ ШЉАКЕ

NA YANG, PING NING, KAI LI и JUNYA WANG

*Faculty of Environmental Science and Engineering, Kunming University of Science and Technology,
Kunming, 650500, Yunnan, P. R. China*

Примена калцинисане магнезитне шљаке за уклањање CO₂ је нови и једноставан метод за истовремени третман CO₂ и шљаке настале при производњи магнезијума. У овом раду је испитивано уклањање CO₂ помоћу калцинисаног магнезита из симулираног влажног димног гаса добијеног мешањем CO₂ и водене паре. Калцинисана магнезитна шљака је показала одличне перформансе као адсорбент CO₂, капацитета 3,01 mmol/g CO₂, који се смањује на 2,18 mmol/g након 8 циклуса адсорпције/десорпције, што је супериорније у односу на магнезит. За карактеризацију магнезитне шљаке коришћене су следеће методе: XRF, FT-IR, TG-DSC, XRD, CO₂-TPD и BET. Помоћу XRF анализе показано је да су главне компоненте магнезитне шљаке MgSiO₃ и MgCO₃. Резултати овог рада показују да се калцинисана магнезитна шљака може користити као адсорбент за CO₂.

(Примљено 28. маја, ревидирано 12. септембра, прихваћено 19. септембра 2018)

REFERENCES

1. K. S. Lackner, *Science* **300** (2003) 1677 (<http://dx.doi.org/10.1126/science.1079033>)
2. Z. H. Li, Y. Wang, K. Xu *et al.*, *Fuel Process Technol.* **151** (2016) 101 (<http://dx.doi.org/10.1016/j.fuproc.2016.05.019>)
3. N. Yang, R. Wang, *Hua Gong Xue Bao* **64** (2013) 128 (in Chinese)
4. P. Z. Li, X. J. Wang, Y. X. Li *et al.*, *Micropor. Mesopor. Mat.* **176** (2013) 194 (<https://doi.org/10.1016/j.micromeso.2013.03.052>)
5. X. Xie, Y. J. Li, C. T. Liu *et al.*, *Fuel Process Technol.* **138** (2015) 500 (<http://dx.doi.org/10.1016/j.fuproc.2015.06.028>)
6. W. J. Xie, R. Wang, *Petroleum Coal* **56** (2014) 418 (http://www.vurup.sk/wp-content/uploads/dlm_uploads/2017/07/pc_4_2014_wang_318.pdf)
7. N. Yang, R. Wang, *J. Serb. Chem. Soc.* **80** (2015) 265 (<http://dx.doi.org/10.2298/JSC220214103Y>)
8. I. Zamboni, C. Courson, A. Kiennemann, *Appl. Catal., B-Environ.* **203** (2017) 154 (<http://dx.doi.org/10.1016/j.apcatb.2016.10.024>)
9. S. J. Han, Y. Bang, H. J. Kwon, H. C. Lee *et al.*, *Chem. Eng. J.* **242** (2014) 357 (<http://dx.doi.org/10.1016/j.cej.2013.12.092>)
10. S. W. Bian, J. Baltrusaitis, P. Galhotra *et al.*, *J. Mater. Chem.* **20** (2010) 8705 (<http://dx.doi.org/10.1039/C0JM01261K>)
11. H. Vishwanath, S. Raghavendra, G. S. Jeong, *Chem. Eng. J.* **308** (2017) 177 (<http://dx.doi.org/10.1016/j.cej.2016.09.052>)
12. A. Zukal, J. Pastva, J. Cejka, *Micropor. Mesopor. Mat.* **167** (2013) 44 (<http://dx.doi.org/10.1016/j.micromeso.2012.05.026>)
13. M. Bhagiyalakshmi, P. Hemalatha, M. Ganesh *et al.*, *Fuel* **90** (2011) 1662 (<http://dx.doi.org/10.1016/j.fuel.2010.10.050>)
14. X. Jiao, L. Li, N. Zhao *et al.*, *Energy Fuel* **27** (2013) 5407 (<http://dx.doi.org/10.1021/ef401085a>)
15. J. Y. Wang, L. Huang, Q. Z. Zheng *et al.*, *J. Ind. Eng. Chem.* **36** (2016) 255 (<http://dx.doi.org/10.1016/j.jiec.2016.02.010>)
16. J. Y. Wang, X. Y. Mei, L. Huang *et al.*, *J. Energy Chem.* **24** (2015) 127 ([http://dx.doi.org/10.1016/S2095-4956\(15\)60293-5](http://dx.doi.org/10.1016/S2095-4956(15)60293-5))

17. Q. Wang, H. H. Tay, Z. Y. Zhong *et al.*, *Energy Environ. Sci.* **5** (2012) 7526 (<http://dx.doi.org/10.1016/j.jechem.2017.01.003>)
18. J. Y. Wang, Y. Yang, L. Jia, *et al.*, *J. Nanosci. Nanotechnol.* **18** (2018) 2956 (<http://dx.doi.org/10.1166/jnn.2018.14381>)
19. J. Y. Wang, L. Huang, R. Yang *et al.*, *Energy Environ. Sci.* **7** (2014) 3478 (<http://dx.doi.org/10.1039/c4ee01647e>)
20. N. Yang, P. Ning, K. Li *et al.*, *J. Taiwan Inst. Chem., E* **86** (2018) 73 (<https://doi.org/10.1016/j.jtice.2018.02.006>)
21. E. F. Chen, T. Zhang, *Liao Ning Hua Gong* **36** (2007) 363 (in Chinese)
22. C. S. Zhao, Y. Fan, M. H. Xia *et al.*, *Shen Yang Gong Cheng Xue Bao* **4** (2008) 1 (in Chinese)
23. A. Samanta, Z. An, G. K. H. Shimizu *et al.*, *Ind. Eng. Chem. Res.* **51** (2012) 1438 (<http://dx.doi.org/10.1021/ie200686q>)
24. D. Bahamon, L. F. Vega, *Chem. Eng. J.* **284** (2016) 437 (<http://dx.doi.org/10.1016/j.cej.2015.08.098>)
25. Y. H. Kim, V. A. Tuan, M. K. Park *et al.*, *Micropor. Mesopor. Mat.* **197** (2014) 299 (<http://dx.doi.org/10.1016/j.micromeso.2014.06.026>)
26. Z. X. Ling, B. Zheng, Q. L. Du *et al.*, *Solid State Sci.* **13** (2011) 2073 (<http://dx.doi.org/10.1016/j.solidsatatesciences.2010.01.013>)
27. B. Margandan, H. Pushparaj, G. Mani *et al.*, *Fuel* **90** (2011) 1662 (<http://dx.doi.org/10.1016/j.fuel.2010.10.050>)
28. B. Margandan, J. Y. Lee, H. T. Jang, *Int. J. Green Gas Con.* **4** (2010) 51 (<http://dx.doi.org/10.1016/j.ijggc.2009.08.001>)
29. Z. X. Zhao, H. X. Dai, Y. C. Du *et al.*, *Mater. Chem. and Phys.* **128** (2011) 348 (<http://dx.doi.org/10.1016/j.matchemphys.2011.02.073>)
30. K. K. Han, Y. Zhou, W. G. Lin *et al.*, *Micropor. Mesopor. Mat.* **169** (2013) 112 (<http://dx.doi.org/10.1016/j.micromeso.2012.11.004>)
31. H. Zhao, W. Yan, Z. Bian *et al.*, *Solid State Sci.* **14** (2012) 250 (<http://dx.doi.org/10.1016/j.solidstatesciences.2011.11.026>)
32. G. Song, Y. D. Ding, X. Zhu *et al.*, *Colloids Surfaces, A* **470** (2015) 39 (<http://dx.doi.org/10.1016/j.colsurfa.2015.01.061>)
33. A. Zukal, J. Pastva, J. Cejka, *Micropor. Mesopor. Mat.* **167** (2013) 44 (<http://dx.doi.org/10.1016/j.micromeso.2012.05.026>)
34. G. Song, X. Zhu, R. Chen *et al.*, *Chem. Eng. J.* **283** (2016) 175 (<http://dx.doi.org/10.1016/j.cej.2015.07.055>)
35. Y. Sun, J. Zhang, C. Wen *et al.*, *J. Taiwan Inst. Chem., E* **63** (2016) 170 (<http://dx.doi.org/10.1016/j.jtice.2016.02.030>)
36. G. B. Elvira, G. C. Francisco, M. Victor *et al.*, *J. Environ. Sci.-China* **57** (2017) 418 (<http://dx.doi.org/10.1016/j.jes.2016.11.016>)
37. S. Zhang, W. Q. Cai, J. Yu *et al.*, *Chem. Eng. J.* **310** (2017) 216 (<http://dx.doi.org/10.1016/j.cej.2016.10.114>).